Bull. Mater. Sci., Vol. 37, No. 6, October 2014, pp. 1309–1314. © Indian Academy of Sciences.

Heavy lithium-doped ZnO thin films prepared by spray pyrolysis method

M ARDYANIAN* and N SEDIGH

School of Physics and Centre for Solid State Physics Research, Damghan University, 3671641167, Damghan, Iran

MS received 21 July 2013; revised 5 August 2013

Abstract. Lithium-doped ZnO thin films ($ZnO : Li_x$) were prepared by spray pyrolysis method on the glass substrates for x (x = [Li]/[Zn]) value varied between 5 and 70%. Structural, electrical and optical properties of the samples were studied by X-ray diffraction (XRD), UV–Vis–NIR spectroscopy, scanning electron microscopy (SEM), Hall effect and sheet resistance measurements. XRD results show that for $x \leq 50\%$, the structure of the films tends to be polycrystals of wurtzite structure with preferred direction along (0 0 2). The best crystalline order is found at $x = 20\%$ and the crystal structure is stable until $x = 60\%$. The Hall effect results describe that Li doping leads to change in the conduction type from *n*- to *p*-type, again it changes to *n*-type at $x = 70\%$ and is attributed to self-compensation effect. Moreover, the carrier density was calculated in the order of 10^{13} cm^{-3}. The resistivity of Li-doped films decreases until 22 Ω cm at $x = 50\%$. Optical bandgap was reduced slightly, from 3·27 to 3·24 eV as a function of the grain size. Optical transmittance in the visible range reaches $T = 97\%$, by increasing of Li content until $x = 20\%$. Electrical and optical properties are coherent with structural results.

Keywords. ZnO; spray pyrolysis; lithium; XRD; UV–Vis–NIR.

1. Introduction

Zinc oxide (ZnO) is a semiconductor with a wide and direct bandgap equal to 3·37 eV at 300 K, large exciton binding energy (60 meV) and strong luminescence emission in ultraviolet (UV) domain. It has become the second most widely studied material after Si for the past decade, because of its advantages as low material cost, low resistivity, high transparency in the visible range, relatively low deposition temperature and stability in hydrogen plasma (Özgür *et al* 2005). It is presently used in many diverse products, such as piezoelectric transducers, varistors, transparent conducting layers for the photovoltaic industry, optoelectronic application (Soki *et al* 2000; Look *et al* 2004), as well as application in heterostructures for fabrication of photodiodes (Jeong *et al* 2003), diluted magnetic semiconductors (Ando *et al* 2001) and nanopiezotronics (Chen *et al* 2010). ZnO is naturally *n*-type semiconductor because of a deviation from stoichiometry, due to the presence of intrinsic defects such as oxygen vacancies and Zn interstitials (Özgür *et al* 2005). For fabricating the light-emitting diodes, *p–n* junction is needed; known acceptors in ZnO include group-I elements such as lithium (Li) (Bilgin 2009) Na and K, copper (Cu) (Kanai 1991a), silver (Ag), (Kanai 1991b), and group-V elements such as N, P and As. However, the formation of deep acceptor levels, implies not to contribute significantly to *p*-type conduction. It has been believed that the most promising dopants for *p*-type ZnO are the group-V elements, although theory suggests some difficulty in achieving shallow acceptor level. ZnO films have been prepared by different techniques, including spray pyrolysis, sputtering, epitaxy, sol–gel, chemical vapour deposition, molecular beam and evaporation (Gal *et al* 2000; Studenikin *et al* 2000). Among these techniques, spray pyrolysis is a simple and inexpensive method for the preparation ZnO films. In this article, Li doping in a wide range of dopant content was effectuated and its influence on the electrical, structural and optical properties of ZnO thin films investigated.

2. Experimental

Lithium-doped ZnO ($ZnO : Li_x$) thin films were prepared by spray pyrolysis techniques on glass substrates. Before deposition, the substrates were cleaned with normal detergent and deionized distilled water, later they were rinsed with 2-propanol. The spraying set-up consists of a scanning spraying nozzle placed 35 cm apart from the heated substrates with the flow rate of 3 mL/min. The carrier gas was dry air at 3 atmospheres pressure. The substrates were installed on a hot plate rotating at 5 rpm rate. The initial spraying solution was 0·15 mol/L of zinc acetate ($Zn(CH_3COO)_2 \cdot 2H_2O$) in 100 mL solution of water and

*Author for correspondence (ardyanian@du.ac.ir)

2-propanol with 1 : 3 ratio as a solvent. The best spray parameters were determined based on a systematic study as 3 mL/min for deposition rate, 450 °C for substrate temperature and 100 mL for solution volume.

Li doping was done by adding lithium chloride in zinc acetate solution, Li concentration was calculated as; x = [Li]/[Zn] = [LiCl]/[$Zn(CH_3COO)_2$] and its values were chosen between 5 and 70%.

The average thickness of the thin films was around 130 nm, measured utilizing UV–Vis–NIR spectroscopy data and calculating by PUMA software (Birgin *et al* 1999). The sheet resistance (R_s) of the films was measured by two-point probe method using thermally evaporated aluminum electrodes; the resistivity was calculated using the sheet resistance by the following relation

$$\rho = R_s t. \tag{1}$$

Conduction type (n or p) was determined by the Hall effect experiment using a coil of 100 turns for creating the magnetic flux density (B) up to 150 mT, the power supply for creating the longitudinal voltage up to 15 V. The measurement of the Hall voltage (V_H) was done by a microvoltmeter. Also, carriers' density was calculated using the Hall effect results and the following equation (Bagheri-Mohagheghi *et al* 2009)

$$N_{n,p} = \frac{IB}{|q|V_H t}, \tag{2}$$

where I, t and q are the measured current, the thickness of the films, electron charge, respectively. For the structural studies of the films, XRD patterns of ZnO and ZnO : Li_x thin films were recorded by D8 Advance Bruker system using CuKα ($\lambda = 0{\cdot}15406$ nm) radiation. The average crystallite size, D, was calculated using the Scherrer's formula (Bagheri-Mohagheghi *et al* 2008)

$$D = \frac{k\lambda}{\beta \cos\theta}, \tag{3}$$

where β is the full-width at half-maximum (FWHM) of the corresponding XRD peak at radiant, k is correction factor ($\approx 0{\cdot}9$) which is correlated to the shape of nanocrystals, considering the spherical shape. λ is X-ray wavelength ($\lambda_{Cuk\alpha} = 0{\cdot}15406$ nm) and θ the Bragg diffraction angle. Surface morphology of the films was observed by Philips XL-30 SEM system. The optical measurements were carried out in the range of 190–1100 nm using Unico 4802 spectrophotometer system. The direct bandgap (E_g) of the prepared films was obtained from the extrapolation of the linear part of the $(\alpha h\nu)^2$ curve vs photon energy ($h\nu$) and using the Tauc equation (Bagheri-Mohagheghi *et al* 2008)

$$(\alpha h\nu)^2 = A(h\nu - E_g), \tag{4}$$

where α and E_g are the absorption coefficient and the bandgap energy, respectively, and A is a constant.

3. Results and discussion

3.1 *Structural properties*

3.1a *XRD results*: According to the procedure described in the previous section, figure 1 represents XRD patterns of ZnO : Li_x thin films as a function of Li concentration. As illustrated, the spectra describe the wurtzite polycrystal structure with preferred orientation along (0 0 2). Diffraction peak angle of (0 0 2) planes for ZnO bulk single crystal is 34·42° (JCPDS 0361451 and 40831); this peak lies at 34·57° for undoped ZnO film of our samples. This shift to higher angles could be attributed to residual stress in ZnO thin films which causes the decrease in the inter-planar distance of the lattice.

By increasing the Li content (x), a variation on the diffraction peak angle of (0 0 2) planes is observed; the peak centre shifts to lower and higher angles alternatively as a function of x (table 1). This implies a competition between tensile and compressive stress in the lattice that

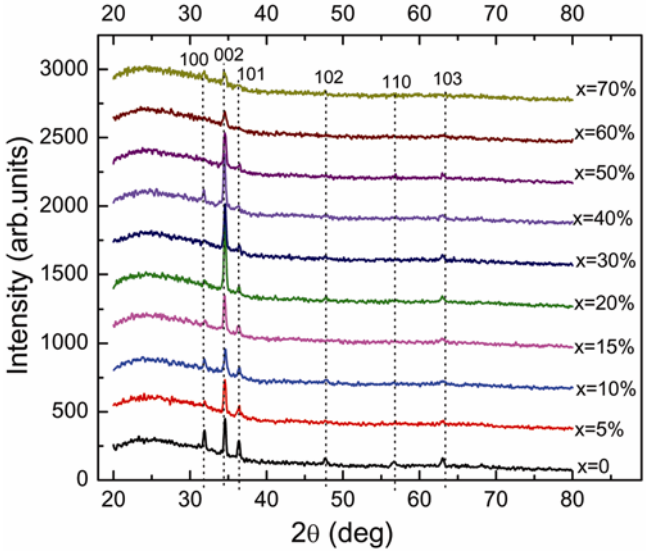

Figure 1. XRD pattern of ZnO : Li_x thin film as a function of Li concentration.

Table 1. XRD parameters of ZnO : Li_x thin films for different Li concentration.

Li content (x at%)	2θ (°)	Interplanar distance (Å)	FWHM (°)	Mean grain size (nm)
0	34·59	2·591	0·280	29·72
5	34·55	2·594	0·298	27·92
10	34·60	2·591	0·279	29·80
15	34·49	2·598	0·287	29·00
20	34·55	2·594	0·267	31·17
30	34·59	2·591	0·248	33·56
40	34·50	2·601	0·260	32·01
50	34·58	2·592	0·276	30·13
60	34·50	2·597	0·380	21·90

may be caused by substitution of Li atoms at the interstitial and Zn sites, respectively (Zeng *et al* 2005; Bilgin 2009). A decrease of FWHM and variation of the intensity of the (0 0 2) peaks, in comparison with undoped ZnO films, are observed for $x \geq 20\%$ and $x < 50\%$, respectively. Increase of (0 0 2) peak intensity (table 1) could be attributed to improve the crystallinity due to decreasing number of defects and increasing crystallites size; it could also be due to modification of nanocrystal growing process as a catalyser (Chu *et al* 2010). Decrease in the peak intensity is attributed to substitution of Li^+ ions with ionic radius = 0·68 Å to Zn^{2+} ions with ionic radius = 0·74 Å as reported by other researchers (Bilgin 2009). For $50\% \leq x \leq 70\%$, the intensity of the (0 0 2) peak decreases and the other diffraction peaks almost disappear. This is attributed to incorporation of more Li atoms that causes the increase in the density of more Li atoms in the interstitial sites; hence, the insoluble Li atoms are segregated at the grain boundaries and they suppress the growth of $ZnO : Li_x$ crystals (Nayak *et al* 2009). It is noted that the crystal structure of $ZnO : Li_x$ thin films is stable up to Li content of 70%, which may be an advantage for the thin films prepared by spray pyrolysis method.

3.1b *SEM images*: The images of scanning electron microscopy (SEM) are represented in figure 2. An evolution in the morphology of the surfaces is observed as a function of Li content. The graining was modified for x up to 20% and the grains are well separated. At $x = 40\%$ the large clusters were formed on the surface which has taken place by nucleation and coalescence of the grains at high Li content. It is assured that Li doping in ZnO influences nucleation density that both nucleation sites and the number of nuclei increase with increasing Li ion (Mohamed *et al* 2005; Lin *et al* 2007). It is confirmed in the figure 2(e and f) corresponding to $x = 50$ and 60% in which the grains are well coalesced. For $x = 70\%$ (figure 2g), the sample is almost amorphous with a uniform and continuous surface. This is in coherence with XRD results and could be due to increase in the density of Li atoms in interstitial sites, which leads to segregate the insoluble Li atoms at the grain boundaries and suppress the growth of $ZnO : Li_x$ crystals (Nayak *et al* 2009).

3.2 *Optical properties*

3.2a *Transmittance*: Figure 3 shows transmittance of $ZnO : Li_x$ thin films vs wavelength and in different Li contents, x. As illustrated, for $10\% < x \leq 20\%$, transmittance of Li-doped films in the range of 400–550 nm increases by increasing the Li content and becomes greater than undoped ZnO films. This could be attributed to decrease in the number of defects and increasing the crystalline order after Li doping. For higher values of x, transparency slightly decreases, since most of the Li ions are located in interstitial sites of the atomic planes, the reduction of transparency could be attributed to dispersion of the visible light due to incorporation of Li atoms in the interstitial sites (Meyer *et al* 2007). Nevertheless, XRD results describe (figure 1), for $40\% \leq x \leq 60\%$, unless (0 0 2) diffraction peak, other peaks are almost suppressed, which could be a reason for decreasing light dispersion and increasing transparency in this range of Li content.

3.2b *Bandgap energy*: Optical bandgap of the thin films can be obtained by extrapolation of the curves based on (4). As illustrated in figure 4, all of the doped thin films generally represent a bandgap narrowing about 0·02 eV compared with undoped ZnO thin film; this low reduction could be explained by the growth of the grain size, which are been in table 1 and observed in SEM images. For $x = 5\%$, in spite of reduction of grains size, a bandgap narrowing is observed; it could be attributed to the local electric fields due to impurity, disorder or any other defects which lead to affect the band tails near the band edge (Bilgin 2009). For $x > 5\%$, a bandgap widening is observed; The bandgap of ZnO is particularly sensitive to small changes in carrier concentration, grain boundary configuration and film stress as reported in the literature (Srikant and Clarke 1997, 1998). Also, the bandgap value of ZnO films generally increases with Li doping, which converts the shallow donor Zn sublevels to deep-sublevels below the conduction band (Sberveglieri *et al* 1992; Mohamed *et al* 2001) as represented in the inset of figure 4 for $x < 50\%$, another reason for increase of the bandgap could be the Burstein–Moss (B–M) effect (Bin *et al* 2009). While for heavy Li-doped thin films ($x > 50\%$) there is an evident narrowing of the bandgap, which could be attributed to the combined effect of the conduction-band renormalization (Bin *et al* 2009).

3.3 *Electrical properties: Hall effect and sheet resistance*

Hall effect experiments were done for determining the conduction type of semiconductor and also the carrier density. Table 2 and figure 5 represent the results of Hall effect and sheet resistance measurements as a function of x. Li-doped samples are p-type semiconductors for $x \leq 60\%$ and carrier density is found in the order of 10^{13} cm^{-3}. At $x = 70\%$, p-type conduction changes to n-type again. Resistivity decreases continuously and reaches a minimum at $x = 50\%$, it increases at $x = 60\%$ and decreases again at $x = 70\%$. The generation of p-type ZnO film is due to substitution of acceptor Li ions for Zn ions (Zeng *et al* 2006). The maximum solubility of Li is estimated to be 10^{19} cm^{-3} under O-rich conditions (Lee and

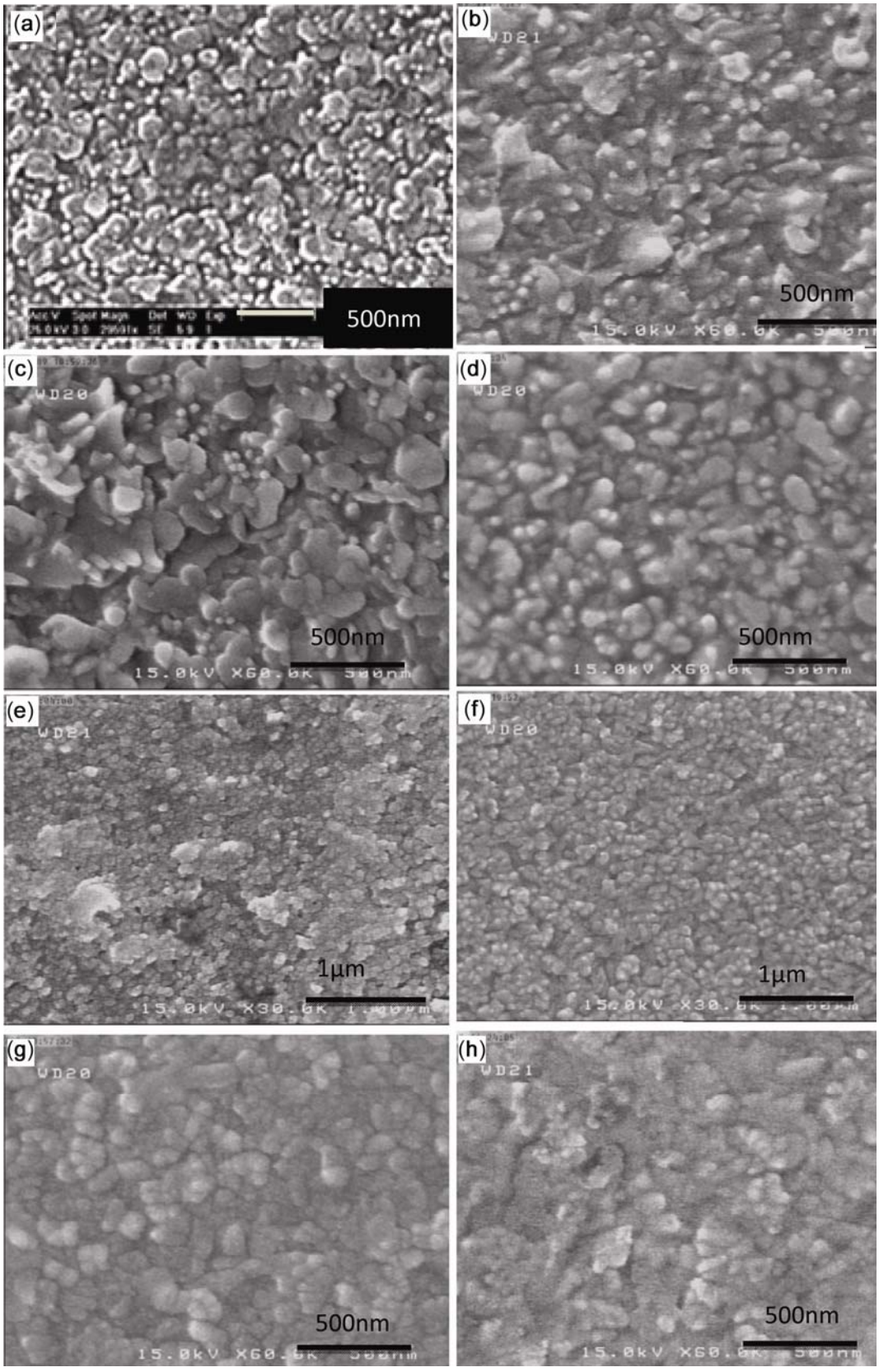

Figure 2. SEM images of ZnO : Li_x thin films for different Li concentrations. (**a**) Undoped ZnO, (**b**) $x = 5\%$, (**c**) $x = 10\%$, (**d**) $x = 20\%$, (**e**) $x = 40\%$, (**f**) $x = 50\%$, (**g**) $x = 60\%$ and (**h**) $x = 70\%$.

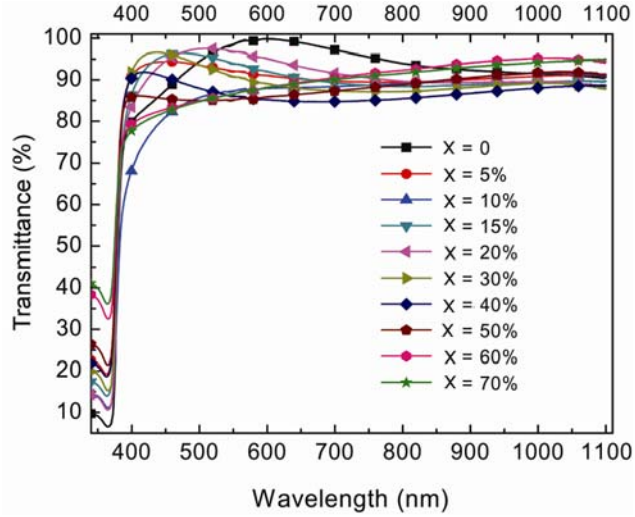

Figure 3. Transmittance curves of $ZnO:Li_x$ thin films as a function of lithium content (x).

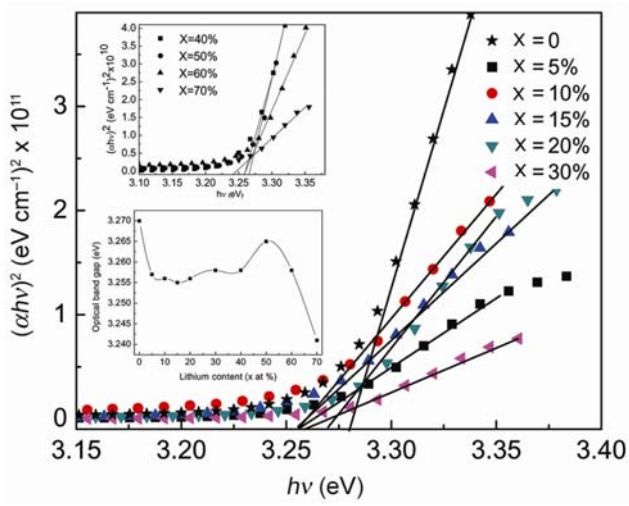

Figure 4. Optical bandgap of $ZnO:Li_x$ thin films as a function of lithium content (x); down inset: Bandgap evolution vs Li content.

Table 2. The results of Hall effect and sheet resistance measurements as a function of x.

Li content (x at%)	Semiconductor type	Carrier density (cm^{-3}) × 10^{13}	Sheet resistance (MΩ/□)	Resistivity (ρ) (Ω cm)
0	*n*	4·28	8·1	102
5	*p*	6	4	64
10	*p*	34·2	3·3	49
15	*p*	6	6	54
20	*p*	13·2	3·8	30
40	*p*	1·3	3·9	44
50	*p*	0·5	15	22
60	*p*	3	33	310
70	*n*	29	1·4	23

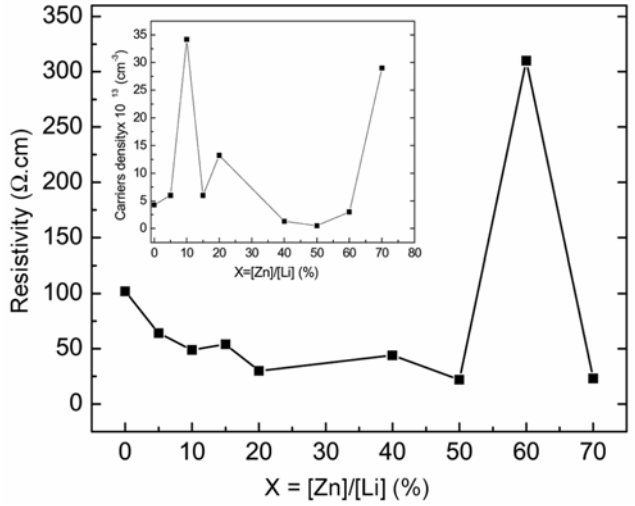

Figure 5. Resistivity and carrier density (inset) as a function of Li content.

Chang 2006), which corresponds to low values of x in our samples. For higher values of Li content ($x = 70\%$) excess of highly mobile Li ions incorporated in interstitial sites as donor defect (self-compensation effect) leads to change of conduction type to *n* (Lander 1960; Lee and Chang 2006; Meyer *et al* 2007). As seen in table 2, the carriers density at $x = 10\%$ is more than $x = 20\%$, while resistivity at $x = 10\%$ is more than at $x = 20\%$. It is attributed to quality of the surface (figures 2b and c); at $x = 20\%$ the grains are more coalesced and their sizes are uniform, while at $x = 10\%$ the grains are well separate with diverse sizes, which leads to the increase of carriers dispersion in the grains boundaries and resistivity as well. General decrease of the resistivity for $x < 60\%$ is attributed to increase in holes density; this leads to the suppression of intrinsic donor defects and modification of the crystalline structure as observed in XRD results (figure 1). Increase of resistivity for heavy doping ($x = 60\%$) is attributed to carrier scattering by Li ions incorporated in interstitial sites and they play the role of donor defects. At $x = 70\%$, conduction type changes to *n*-type and carrier density increases (table 2) and resistivity decreases again (figure 5); regarding microscopy images (figure 2e), at $x = 70\%$, grain boundaries are suppressed and the surface becomes uniform and continuous due to segregation of insoluble Li atoms at grain boundaries. This leads to suppression of

electrons scattering in grain boundaries and the resistivity reduction.

4. Conclusions

In this work, the influence of Li doping on the structural, optical and electrical properties of ZnO thin films for a wide range of Li content was investigated. It is found that, up to 50% of Li content, the structure is wurtzite polycrystal with preferred orientation along (0 0 2). The crystal structure is stable for x up to 70%. A low bandgap narrowing was observed, which was attributed to growing of the grains. Carriers density and resistivity were measured and found in the order of 10^{13} cm^{-1} and about 40 Ω cm, respectively, that resistivity generally decreases by Li doping. The samples have the best transmittance in the visible range for Li content up to 20%. This is attributed to modification of the crystalline structure and suppression of the intrinsic defects. $ZnO:Li_x$ thin films have p-type conduction, which change to n-type at $x = 70\%$; this effect is attributed to self-compensation effect of lithium atoms, incorporated in interstitial sites of the lattice. As a result, p-type conduction, high transparency in the visible range, excellent crystal stability and low resistivity for doping up to 70% are the advantages of $ZnO:Li_x$ thin films prepared by spray pyrolysis method. Hence, it is a good substitution candidate for TCO materials and fabrication of p–n junctions based on ZnO.

Acknowledgements

This work was supported financially by the Research Council of Damghan University in I R Iran (Grant No. 7035). The authors also wish to acknowledge Dr M M Bagheri-Mohagheghi for technical and scientific support of this work.

References

Ando K, Saito H, Jin Z, Fukumura T, Kawasaki M, Matsumoto Y and Koinuma H 2001 *J. Appl. Phys.* **89** 7284

Bagheri-Mohagheghi M M, Shahtahmasebi N, Alinejad M R, Youssefi A and Shokooh-Saremi M 2008 *Phys. B: Condens. Matter* **403** 2431

Bagheri-Mohagheghi M M, Shahtahmasebi N, Alinejad M R, Youssefi A and Shokooh-Saremi M 2009 *Solid State Sci.* **11** 233

Bin W, Yue Z, Jiahua M and Wenbin S 2009 *Appl. Phys.* **A94** 715

Birgin E G, Chambouleyron I and Martınez J M 1999 *J. Comput. Phys.* **151** 862

Bilgin V 2009 *J. Electron. Mater.* **38** 1969

Chen Y Q, Zheng X J, Mao S X and Li W 2010 *J. Appl. Phys.* **107** 094302

Chu H, Wei L, Cui R, Wang J and Li Y 2010 *Coordination Chem. Rev.* **254** 1117

Gal D, Hodes G, Lincot D and Schock H W 2000 *Thin Solid Films* **361** 79

Jeong I S, Kim J H and Im S 2003 *Appl. Phys. Lett.* **83** 2946

Joint Committee on Powder Diffraction Standards, Powder Diffraction File, (Philadelphia, PA: ASTM, 1967). Card 0361451 (for ZnO hexagonal) and 40831 (for Zn hexagonal)

Kanai Y 1991a *Jpn. J. Appl. Phys.* **30** 703

Kanai Y 1991b *Jpn. J. Appl. Phys.* **30** 2021

Lee E C and Chang K J 2006 *Phys. B: Condens. Matter* **376** 707

Lander J J 1960 *J. Phys. Chem. Solids* **15** 324

Lin W, Ma R, Shao W and Liu B 2007 *Appl. Surf. Sci.* **253** 5179

Look D C, Claflin B, Alivov Y I and Park S J 2004 *Phys. Status Solidi (A)* **201** 2203

Meyer B K, Stehr J, Hofstaetter A, Volbers N, Zeuner A and Sann J 2007 *Appl. Phys.* **A88** 119

Mohamed G A, Abd El-Moiz A B and Rashad M 2005 *Phys. B: Condens. Matter* **370** 158

Mohamed G A, Mohamed E M and Abu El-Fadl A 2001 *Phys. B: Condens. Matter* **308** 949

Nayak P K, Jang J, Lee C and Hong Y 2009 *Appl. Phys. Lett.* **95** 193503

Özgür U, Alivov Y I, Liu C, Teke A, Reshchikov M A, Dogan S and Morkoc H 2005 *J. Appl. Phys.* **98** 041301

Sberveglieri G Groppelli S, Nelli P, Quaranta F, Valentini A and Vasanelli L 1992 *Sens. Actuators B: Chem.* **7** 747

Soki T T, Hatanaka Y and Look D C 2000 *Appl. Phys. Lett.* **76** 3257

Studenikin S A, Golego N and Cocivera M 2000 *J. Appl. Phys.* **87** 2413

Srikant V and Clarke D R 1998 *J. Appl. Phys.* **83** 5447

Srikant V and Clarke D R 1997 *J. Mater. Res.* **12** 1425

Zeng Y J, Ye Z Z, Xu W Z, Chen L L, Li D Y, Zhu L P and Hu Y L 2005 *J. Cryst. Growth* **283** 180

Zeng Y J, Ye Z Z, Xu W Z, Li D Y, Lu J G, Zhu L P and Zhao B H 2006 *Appl. Phys. Lett.* **88** 2172743